Inorganic Chemistry

Article

pubs.acs.org/IC

Rapid, Large-Scale, Morphology-Controllable Synthesis of YOF:Ln^{3+} (Ln = Tb, Eu, Tm, Dy, Ho, Sm) Nano-/Microstructures with Multicolor-Tunable Emission Properties

Yang Zhang,[†,‡] Dongling Geng,[†,‡] Xiaojiao Kang,[†,‡] Mengmeng Shang,[†,‡] Yuan Wu,[†,‡] Xuejiao Li,[†,‡] Hongzhou Lian,[†] Ziyong Cheng,[†] and Jun Lin*[,†]

[†]State Key Laboratory of Rare Earth Resource Utilization, Changchun Institute of Applied Chemistry, Chinese Academy of Sciences, Changchun 130022, People's Republic of China

[‡]University of Chinese Academy of Sciences, Beijing 100049, People's Republic of China

Supporting Information

ABSTRACT: YOF:Ln^{3+} (Ln = Tb, Eu, Tm, Dy, Ho, Sm) nano-/microstructures with a variety of novel and well-defined morphologies, including nanospheres, nanorod bundles, and microspindles, have been prepared through a convenient modified urea-based homogeneous precipitation (UBHP) technique followed by a heat treatment. The sizes and morphologies of the YOF products could be easily modulated by changing the pH values and fluoride sources. XRD, TG-DTA, FT-IR, SEM, and TEM, as well as photoluminescence (PL) and cathodoluminescence (CL) spectra, were used to characterize the prepared samples. The YOF:Ln^{3+} nanospheres show the characteristic f−f transitions of Ln^{3+} (Ln = Tb, Eu, Tm, Dy, Ho, Sm) ions and give bright green, red, blue, yellow, blue-green, and yellow-orange emission, respectively, under UV light and low-voltage electron beam excitation. Furthermore, YOF:0.03Tb^{3+} phosphors exhibit green luminescence with superior properties in comparison with the commercial phosphor ZnO:Zn to a degree, which is advantageous for improving display quality. Because of the simultaneous luminescence of Ln^{3+} in the YOF host, the luminescence colors of YOF:Ln^{3+} phosphors can be precisely adjusted by changing the doped Ln^{3+} ions and corresponding concentrations, which makes these materials hold great promise for applications in field-emission displays.

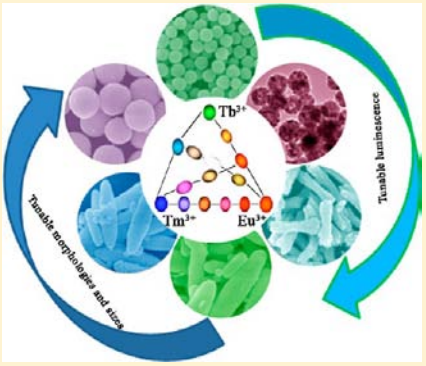

INTRODUCTION

Recently, rare earth ion (Ln^{3+}) doped phosphors have aroused fast growing interest on the basis of their intra-4f or 5d−4f transitions, due to the wide range of applications in lighting and display fields, such as white light emitting diodes (WLEDs), cathode ray tubes (CRTs), plasma display panels (PDPs), vacuum fluorescent displays, and field emission displays (FEDs).[1−6] In particular, WLEDs represent a promising solid-state lighting approach because of the merits of high efficiency, energy savings, environmental friendliness, and long lifetime.[4,7,8] On the other hand, with fascinating features such as thin panel, wide viewing, low power consumption, etc., field emission displays (FEDs) has been considered as one of the most promising next-generation flat panel display techniques.[5,9] Therefore, in order to improve the performance of lighting and display devices, it is urgent to explore novel phosphors with high luminescence efficiency and good chemical durability. Moreover, phosphors of smaller size are highly desired because of the merit of improving resolution by decreasing pixel size.[10−12] Actually, it is necessary to synthesize phosphors with an ideally spherical shape, a narrow size distribution, and nonagglomeration, because spherical phosphors will lead to high packing densities, low scattering of light, high brightness, and high resolution.[13] However, the mechanical grinding method which is conventionally used to decrease the particle size easily results in the formation of large amounts of surface defects, which provides a nonradiative recombination process and ultimately decreases the luminescent efficiency.[5] Thus, it is still a challenge and urgent task to establish an efficient method to synthesize size- and morphology-controlled nano-/micro-luminescent materials with simple, green, economical, and mass production.

Because of their low phonon energy, high ionicity, and high chemical and thermal stability, lanthanide oxyfluorides (LnOFs) have aroused extensive interest for applications in biosensing, optical nanodevices, field-emission-driven phosphors, X-ray detectors, and efficient solar cells.[14−18] Up to now, several techniques have been employed for the synthesis of LnOFs, such as high-temperature-based solid-state reactions and hydrothermal, precipitation, molten salt, electrospinning, and thermolysis methods.[14,19−22] However, these processes suffer from drawbacks such as large crystallites or low yield, long reaction time, and high environment loads, which severely hinder their practical applications.[23] Considering these circumstances, we present the preparation of nano-/microstructures of

Received: June 14, 2013
Published: November 6, 2013

   dx.doi.org/10.1021/ic401501t | Inorg. Chem. 2013, 52, 12986−12994

Table 1. Summary of Experiment Parameters, Morphologies, and Sizes of the As-Prepared YOF

sample	pH	[urea]/[Ln^{3+}]	F^-	calcination temp (°C)	morphology	length	diameter (nm)
Y_2O_3	2	50	none	600	nanospheres		600
YOF	2	50	KF	600	nanospheres		170
YOF	4	50	KF	600	nanospheres		60
YOF	2	50	NH_4F	700	nanorod bundles	700 nm	200
YOF	2	50	LiF	700	microspindles	2−2.5 μm	400−500
					nanospheres		50
YOF	2	50	NaF	700	microspindles	2−2.5 μm	400−500
					nanospheres		50

a YOF phosphor with good dispersion by a modified urea-based homogeneous precipitation (UBHP) technique followed by a heat treatment. In comparison with previous reports, two merits of our method are outstanding. First, our process is environmentally benign without adding any chelating agents and organic solvent. Second, the precipitation method has been proven to be one of the most convenient, efficient, and facile methods for achieving single-phase nano- or microcrystals with well-defined morphology at relatively lower temperature, shorter reaction time, and easier mass production. By the UBHP method, the morphologies (nanospheres, nanorod bundles, and microspindles) and sizes of the as-prepared YOF nano/microstructures could be easily adjusted by changing the species of F^- sources and pH values. Moreover, an exhaustive study of the photoluminescence (PL) and cathodoluminescence (CL) properties of YOF:Ln^{3+} (Ln = Tb, Eu, Tm, Dy, Ho, Sm) phosphors has shown that these materials hold great promise for application in FEDs.

EXPERIMENTAL SECTION

Materials. $Ln(NO_3)_3$ aqueous solutions were obtained by dissolving the corresponding Ln_2O_3 (Ln = Eu, Tm, Dy, Ho, Sm) and Tb_4O_7 (99.999%) in dilute HNO_3 solution with heating and agitation. Other chemicals were purchased from Beijing Chemical Co. All chemicals were of analytical grade and were used directly without further purification.

Preparation. With magnetic stirring, 1 mmol of KF and a certain quantity of $CO(NH_2)_2$ was added to 100 mL of an aqueous solution containing 1 mmol of $Y(NO_3)_3$. Then, dilute HNO_3 was introduced rapidly into the vigorously stirred solution until pH 2 and the beaker was wrapped with polyethylene film. The mixture was heated to 90 °C for 3 h after magnetic stirring for 15 min. The resulting white precipitates were collected by centrifugation, washed several times with deionized water and ethanol, and finally dried at 85 °C in air for 12 h. The final YOF products were retrieved through a heat treatment of the precursors at 600 °C in air for 3 h with a heating rate of 1 °C/min. Other samples were prepared by a similar procedure, except for different F^- sources as well as different pH conditions. The experimental conditions are summarized in Table 1. The doped YOF samples were prepared by introducing the proper amounts of $Ln(NO_3)_3$ instead of $Y(NO_3)_3$ to the solution as described above.

Characterization. The composition and phase purity of the samples were investigated by powder X-ray diffraction (XRD) with a D8 Focus diffractometer (Bruker). Fourier-transform IR spectra were recorded on a PerkinElmer 580B IR spectrophotometer using the KBr pellet technique. The morphology, dimensions, and composition of the as-synthesized nano-/microstructures were examined by means of scanning electron microscopy (SEM, S-4800, Hitachi). Low-/high-resolution transmission electron microscopy (TEM) was performed using a FEI Tecnai G2S-Twin instrument with a field-emission gun operating at 200 kV. Thermogravimetric and differential thermal analysis (TG-DTA) data were recorded with Thermal Analysis Instrument (SDT 2960, TA Instruments, New Castle, DE) with a heating rate of 10°/min in an air flow of 100 mL/min. The photoluminescence (PL) measurements were recorded with a Hitachi F-7000 spectrophotometer, and the cathodoluminescence (CL) measurements were performed in an ultrahigh-vacuum chamber (<10^{-8} Torr), where the phosphors were excited by an electron beams with different voltages and filament currents, and the emission spectra were recorded using an F-7000 spectrophotometer. All of the results were obtained at ambient temperature.

RESULTS AND DISCUSSION

Phase Identification and Morphology. Figure 1a shows the XRD patterns of the as-prepared precursor sample for YOF,

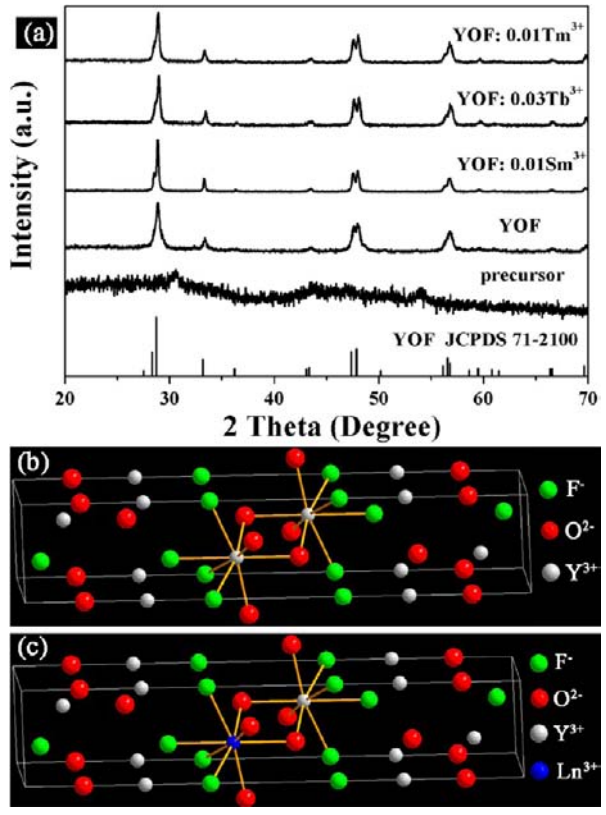

Figure 1. (a) XRD patterns of as-prepared precursor samples, annealed at 600 °C, Ln^{3+}-doped samples, and the standard data of YOF (JCPDS No. 71-2100). Schemes of the rhombohedral phase YOF structures (b) undoped and (c) doped with Ln^{3+} ions.

Ln^{3+}-doped YOF annealed at 600 °C, and the standard data of YOF (JCPDS 71-2100), respectively. There are no obvious diffraction peaks that can be observed from the precursor sample (Figure 1a), which indicates that the sample is amorphous. After calcination at 600 °C, it can be seen that well-defined diffraction peaks can be assigned readily to the rhombohedral phase of YOF, which belongs to the

dx.doi.org/10.1021/ic401501t | Inorg. Chem. 2013, 52, 12986−12994

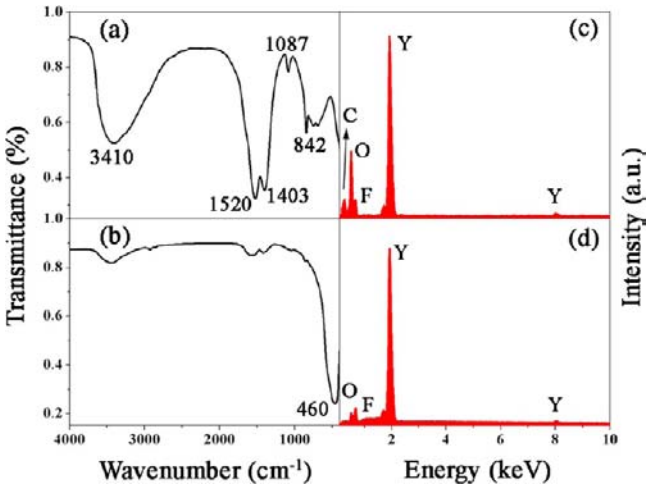

Figure 2. FT-IR spectra of (a) as-prepared precursor samples and (b) YOF obtained by calcining precursor at 600 °C. EDX spectra of (c) as-prepared precursor samples and (d) YOF obtained by calcining the precursor at 600 °C.

rhombohedral crystal system with the $R\bar{3}m$ space group ($a = b = 3.79$ Å, $c = 18.89$ Å).[24] The Y^{3+} cations are coordinated by four O^{2-} and four F^-, all ions occupy the 6-fold 6*c* Wyckoff positions, and the symmetry for Y^{3+} ions is C_{3v}, as is shown in Figure 1b.[25] After doping with Ln^{3+} (Ln = Tb, Eu, Tm, Dy, Ho, Sm) ions, a portion of the Y^{3+} ions will be substituted in the C_{3v} sites (see Figure 1c). No other peaks or impurity phase can be found in the Ln^{3+}-doped samples because of the similar ionic radii and valences of the rare-earth elements.[26]

FT-IR spectroscopy was employed for both the precursor and samples calcined at 600 °C, as displayed in Figure 2. The broad absorption band located at 3410 cm^{-1} can be assigned to the O−H stretching vibration of water. The COO^- and C−F groups generated the bands at 1520 and 1403 cm^{-1} and at 842 and 1087 cm^{-1}, respectively.[5,22] After calcination of the precursor at 600 °C for 3 h, a strong absorption band at 460 cm^{-1} was present, which indicates the formation of YOF.[22,27] The EDX spectra further confirm the conversion process from the precursor sample (Figure 2c) to YOF (Figure 2d) through calcinations. Figure S1 (Supporting Information) shows DSC-TG curves of the as-prepared precursor sample. The mass loss of occlusion water occurs at around 158 °C.[22] The greatest loss of mass occurs at 485 °C because of the crystallization of YOF, which is consistent with the above results.[28]

The SEM and low-/high-resolution TEM images of the precursor and YOF nanospheres prepared at pH 2 with KF as the F^- source are shown in Figure 3. It is obvious that the precursor mainly consists of numerous monodispersed nanospheres with diameter about 200 nm, as displayed in Figure 3a. The SEM image shown in Figure 3b reveals that YOF still maintains the nanosphere morphology except the size is reduced to about 170 nm due to the gradual elimination of C, H, and O through the calcination process.[29] The results of this conversion process are expected to have wide implications for designing morphology-dependent functional compounds.[30−32] Figure 3c,d present the representative TEM images of YOF nanospheres. The obvious lattice fringes confirm the high crystallinity of the samples, as shown in the HRTEM image (Figure 3d). A distance of about 0.163 nm between adjacent lattice fringes could be well assigned as the *d* spacing value of the (116) plane of YOF.

Control experiments demonstrated that pH values and fluoride sources play dominant roles in adjusting the sizes and morphologies of YOF. Control I was to implement the experiments without adding fluoride sources at pH 2, control II was to vary the pH value from 2 to 4, and control III was to prepare YOF in the presence of other fluoride sources such as NH_4F, LiF and NaF instead of KF. It is well-known that Ln^{3+}

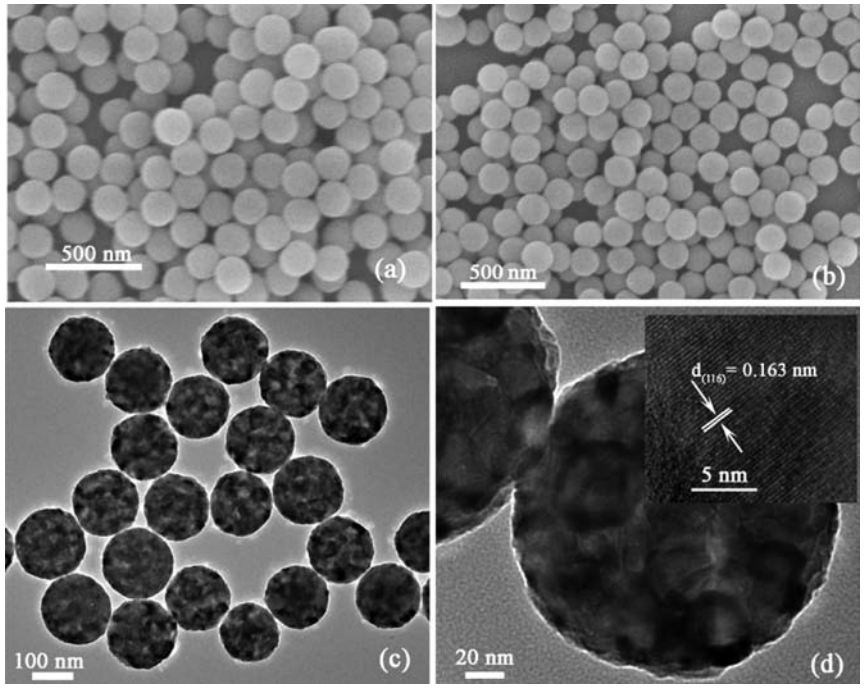

Figure 3. SEM images of the (a) as-prepared precursor samples and (b) YOF obtained by calcining the precursor at 600 °C. (c) TEM and (d) HRTEM images of the YOF samples.

dx.doi.org/10.1021/ic401501t | *Inorg. Chem.* 2013, 52, 12986−12994

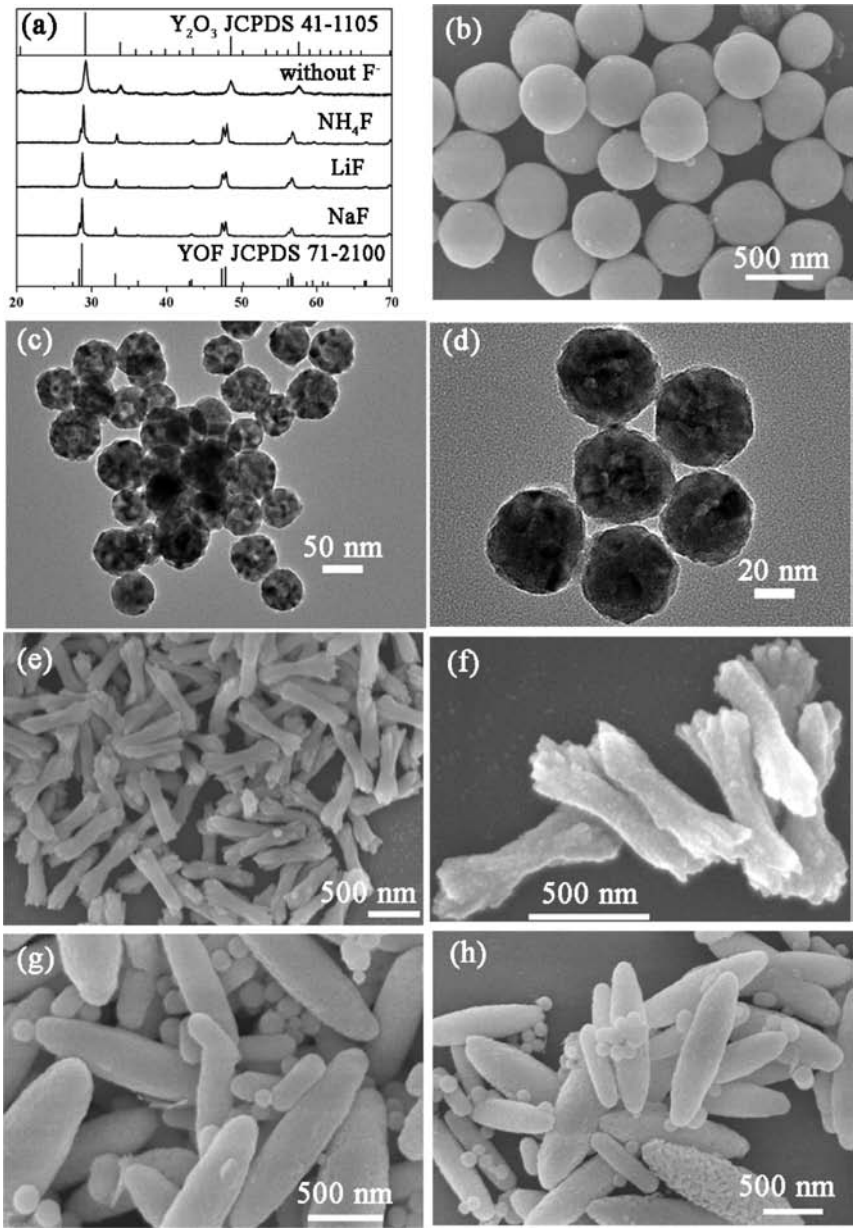

Figure 4. (a) XRD patterns of samples prepared without adding a F^- source and the replacement of KF by NH_4F/LiF/NaF. (b) SEM images of the samples prepared without adding a F^- source. (c, d) Low- and high-magnification TEM images of the YOF samples prepared at pH 4 with KF. (e, f) Low- and high-magnification SEM images of the YOF samples prepared at pH 2 with NH_4F. SEM images of the YOF samples prepared at pH 2 with (g) LiF and (h) NaF.

species are known to precipitate as basic carbonate colloidal spheres of uniform sizes by heating a mixed solution containing Ln^{3+} and a proper amount of urea at temperatures above 83 °C. The precipitating ligands (mainly OH^- and CO_3^{2-}) released from the decomposition of urea precipitated with Ln^{3+} slowly and homogeneously, thus making it possible to obtain monodispersed nanospheres. Then monodispersed colloidal Ln_2O_3 spheres of uniform size and shape could be obtained by calcinations of the precursor.[13,33,34] The products obtained in the control I experiments (without F^- source) are all cubic phases of Y_2O_3, as identified by XRD patterns (Figure 4a), with monodispersed nanospheres of about 600 nm diameter (Figure 4b), which is consistent with previous reports.[13,33] In addition, we could adjust the sizes and morphologies of the particles just by varying the pH values and F^- sources of the initial reaction solution, although the crystal structures of the particles only have the rhombohedral phase of YOF, as shown in Figure 4a. It is obvious that monodispersed and uniform YOF nanospheres with diameters of about 60 nm can be prepared at pH 4, as shown by the TEM micrographs in Figure 4c,d, which are much smaller than the samples prepared at pH 2, in the control II experiments. On the one hand, addition of KF would greatly increase the ionic strength of the reaction medium, and higher ionic strength favors the formation of smaller crystals, in comparison with the products (nanospheres with diameter about 600 nm) prepared via the urea-based homogenerous precipitation method (control I experiments).[35,36] On the other hand, an increase of the pH value to 4 would accelerate the precipitation of Y^{3+} to some extent, thus decreasing the concentration of Y^{3+} and resulting in smaller nanospheres with diameter about 60 nm, in comparison with the samples prepared at pH 2.[34,37,38] As shown in Figure 4e–h, the

dx.doi.org/10.1021/ic401501t | *Inorg. Chem.* 2013, 52, 12986–12994

Scheme 1. Schematic Illustration for the Effects of pH Value and Fluorine Source on the Final Products

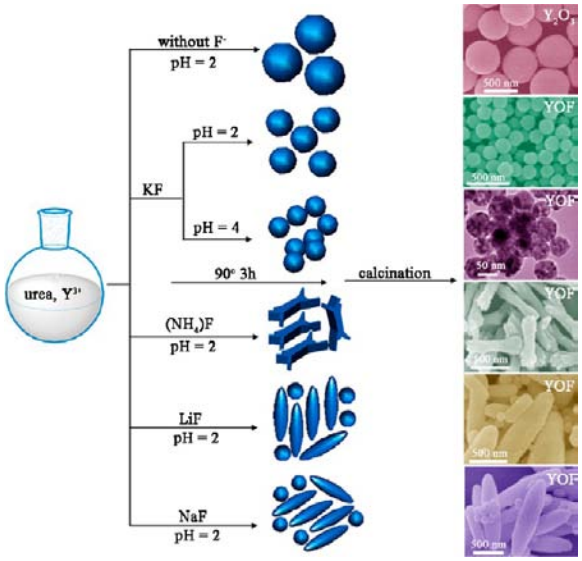

morphologies of the obtained YOF are quite different from those that we have observed in the KF system, when NH_4F, LiF, and NaF were used as the F^- sources, in the control III experiments. Nanorod bundles with a length of about 700 nm

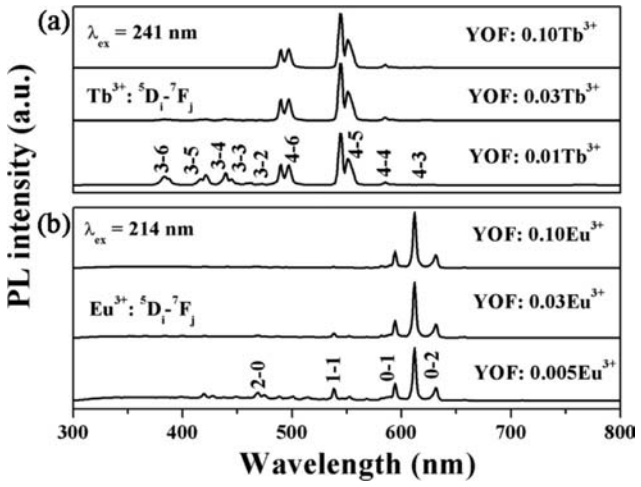

Figure 6. Typical photoluminescence emission spectra of (a) YOF:Tb^{3+} (λ_{ex} 241 nm) and (b) YOF:Eu^{3+} (λ_{ex} 214 nm) with different doping concentrations.

and a diameter of about 200 nm (Figure 4e,f) were obtained through the replacement of KF by NH_4F. For the LiF (Figure 4g) and NaF (Figure 4h) systems, the products are all mainly composed of well-separated microspindles (length about 2−2.5 μm, diameter about 400−500 nm) and nanospheres (diameter about 50 nm). In our system, the cations of K^+, NH_4^+, Li^+, and

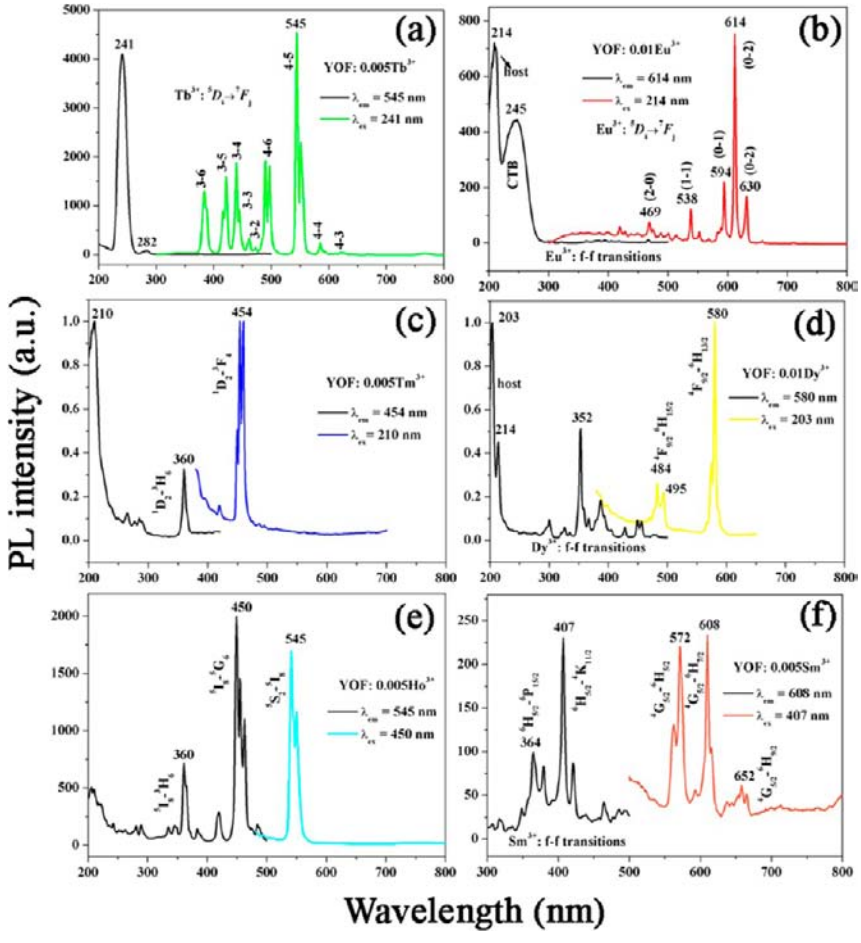

Figure 5. Representative photoluminescence excitation and emission spectra of (a) YOF:0.005Tb^{3+}, (b) YOF:0.01Eu^{3+}, (c) YOF:0.005Tm^{3+}, (d) YOF:0.01Dy^{3+}, (e) YOF:0.005Ho^{3+}, and (f) YOF:0.005Sm^{3+}.

dx.doi.org/10.1021/ic401501t | Inorg. Chem. 2013, 52, 12986−12994

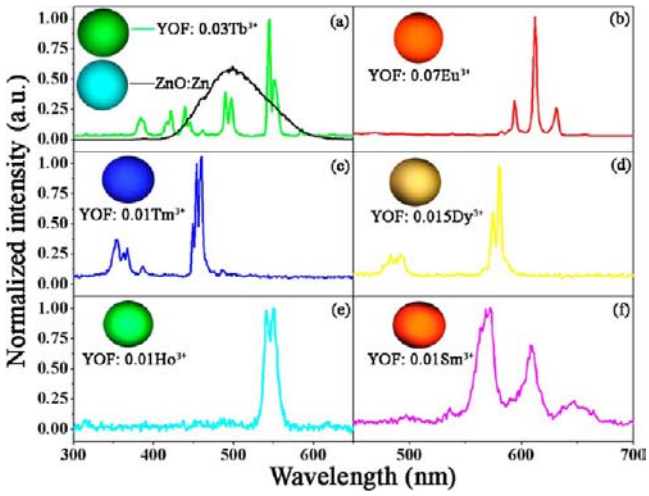

Figure 7. Typical CL spectra of (a) YOF:0.03Tb^{3+} and ZnO:Zn, (b) YOF:0.07Eu^{3+}, (c) YOF:0.01Tm^{3+}, (d) YOF:0.015Dy^{3+}, (e) YOF:0.01Ho^{3+}, and (f) YOF:0.01Sm^{3+}, under low-voltage electron beam excitation (accelerating voltage 3 kV, filament current 90 mA). The insets are their corresponding CL digital photographs.

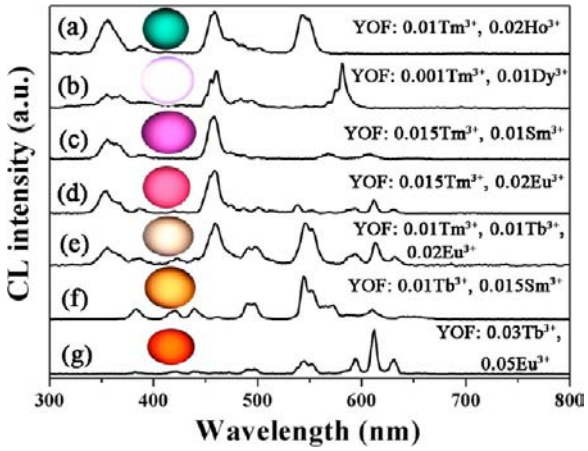

Figure 8. Typical CL spectra of (a) YOF:0.01Tm^{3+},0.02Ho^{3+}, (b) YOF:0.001Tm^{3+},0.01Dy^{3+}, (c) YOF:0.015Tm^{3+},0.01Sm^{3+}, (d) YOF:0.015Tm^{3+},0.02Eu^{3+}, (e) YOF:0.01Tm^{3+},0.01Tb^{3+},0.02Eu^{3+}, (f) YOF:0.01Tb^{3+},0.015Sm^{3+}, and (g) YOF:0.03Tb^{3+},0.05Eu^{3+}, under low-voltage electron beam excitation (accelerating voltage 3 kV, filament current 90 mA). The insets are their corresponding CL digital photographs.

Na^+ could be selectively adsorbed on different surfaces of the initial precursor crystals due to the strong interactions between these cations and OH^-, CO_3^{2-}, and F^- anions during the early stage of the reactions and influence the corresponding surface energy, thus leading to the various morphologies.[36,39,40] An illustration of the formation and morphology evolution of YOF at different pH values and F^- sources is summarized in Scheme 1. In summary, the above results confirm that our method is efficient for synthesizing size- and morphology-controlled nano-/microluminescent materials with simple and mass production.

Photoluminescence Properties. Figure 5 presents the PL excitation and emission spectra of the as-formed YOF:Ln^{3+} (Ln = Tb, Eu, Tm, Dy, Ho, Sm) nanospheres with a diameter of about 170 nm. Generally, the emission properties of Tb^{3+} ions are mainly due to the transitions $^5D_3 \rightarrow {}^7F_J$ in the blue region

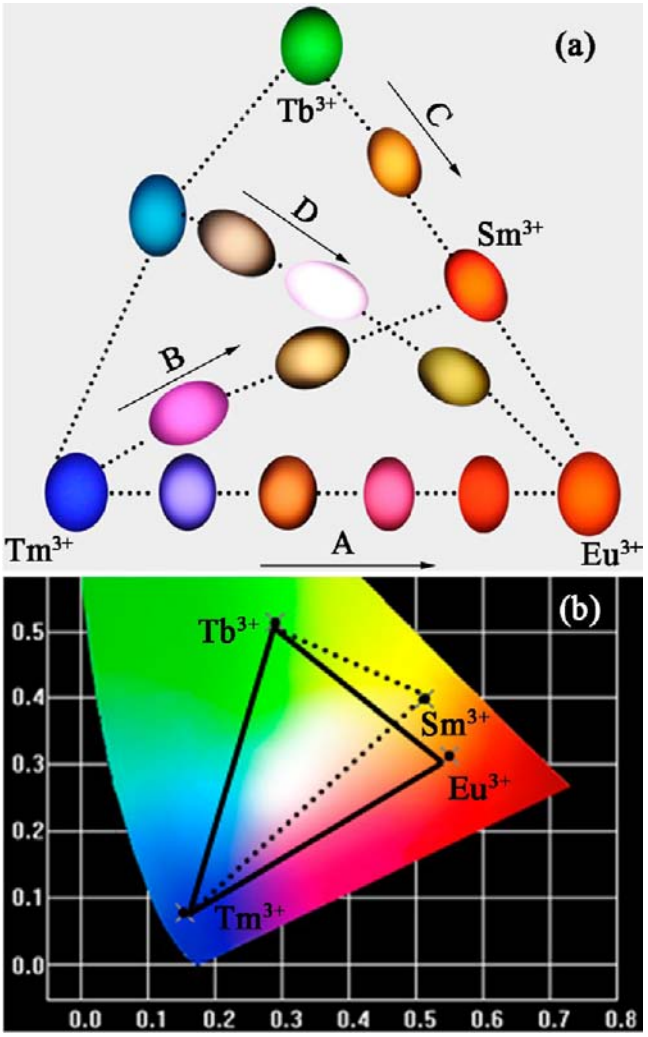

Figure 9. (a) CL digital photographs of YOF:xEu^{3+} (Sm^{3+}), yTb^{3+},zTm^{3+} nanosphere samples annealed at 600 °C. Arrows A–D represent the codoping of Tm^{3+}/Eu^{3+}, Tm^{3+}/Sm^{3+}, Tb^{3+}/Sm^{3+}, and $Tm^{3+}/Tb^{3+}/Eu^{3+}$ in the YOF host, respectively. (b) Solid-lined triangle and dash-lined triangle depicting the tunable color regions of YOF:$Tm^{3+}/Tb^{3+}/Eu^{3+}$ and YOF:$Tm^{3+}/Tb^{3+}/Sm^{3+}$ phosphors, respectively.

and $^5D_4 \rightarrow {}^7F_J$ in the green region (J = 6–2), depending on its doping concentration.[41] It is well-known that the ground state of the Tb^{3+} ion with a $4f^8$ electron configuration is on the $^7F_6$ level, and its $4f^75d^1$ excitation levels have high-spin (HS) ^9D_J and the low-spin (LS) ^7D_J states. The excitation spectrum shows a strong broad band (λ_{max} 241 nm) with a shoulder at about 282 nm, with monitoring of the wavelength at 545 nm, which are due to a spin-allowed $4f^8 \rightarrow 4f^75d$ ($^7F_6$–^7D_J) transition and a spin-forbidden $4f^8 \rightarrow 4f^75d$ ($^7F_6$–^9D_J) transition of Tb^{3+} ions, respectively. The energy difference between these two transitions is around 6000 cm^{-1}, which is consistent with previous reports.[42,43] Under 241 nm UV radiation excitation, the as-prepared YOF:0.005Tb^{3+} shows blue emission peaks at 381, 420, 439, 460, and 472 nm due to the $^5D_3 \rightarrow {}^7F_J$ (J = 6–2, respectively) transitions. The $^5D_4 \rightarrow {}^7F_J$ (J = 6–3) transitions result in green emission lines at 495, 545, 585, and 625 nm, respectively. With an increase of Tb^{3+} concentration, the cross relaxation (Tb^{3+}: $^5D_3 + {}^7F_6 \rightarrow {}^5D_4 + {}^7F_0$) becomes dominant and thus enhances green emission,

dx.doi.org/10.1021/ic401501t | Inorg. Chem. 2013, 52, 12986–12994

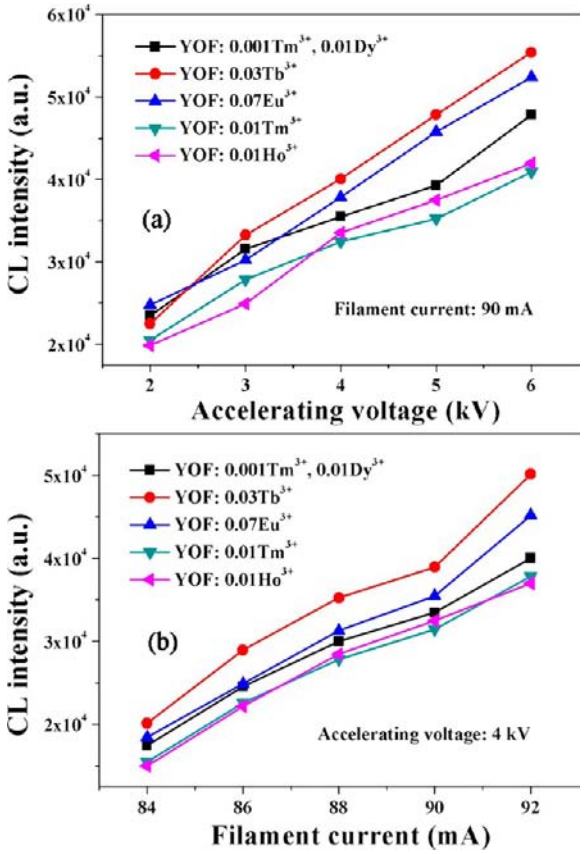

Figure 10. CL intensities of YOF:0.001Tm^{3+},0.01Dy^{3+}, YOF:0.03Tb^{3+}, YOF:0.07Eu^{3+}, YOF:0.01Tm^{3+}, and YOF:0.01Ho^{3+} as a function of (a) accelerating voltage and (b) filament current.

which can be proved by the PL spectrum (Figure 6a) and the CIE coordinates (Figure S2, Supporting Information) for YOF:Tb^{3+} samples with different doping concentrations.

As is known, the characteristic emissions of Eu^{3+} ion result from the transitions $^5D_{0,1,2} \rightarrow {}^7F_J$ (J = 0–4).[44] On moitoring with the wavelength of 614 nm, the excitation spectrum of YOF:0.01Eu^{3+} (Figure 5b) shows a strong band with a maximum at 214 nm ascribed to the host absorption, which could be confirmed by the diffuse reflectance spectrum of YOF shown in Figure S3 (Supporting Information). In addition, the latter broad band with a maximum at 245 nm is assigned to the charge transfer transition of $O^{2-} \rightarrow Eu^{3+}$; in addition, the sharp peaks beyond 350 nm are the characteristic f → f transitions of Eu^{3+} within its $4f^6$ configuration.[5] Upon excitation at 214 nm, YOF:0.01Eu^{3+} samples show all of the transitions $^5D_{0,1,2} \rightarrow {}^7F_J$ of Eu^{3+}, i.e., $^5D_2 \rightarrow {}^7F_0$ (469 nm), $^5D_2 \rightarrow {}^7F_2$ (487 nm), $^5D_2 \rightarrow {}^7F_3$ (515 nm), $^5D_1 \rightarrow {}^7F_1$ (538 nm), $^5D_1 \rightarrow {}^7F_2$ (550 nm), $^5D_0 \rightarrow {}^7F_1$ (594 nm), and $^5D_0 \rightarrow {}^7F_2$ (614 and 630 nm). The emission spectrum is dominated by the hypersensitive transition ($^5D_0 \rightarrow {}^7F_2$) of Eu^{3+}, basically agreeing well with the crystal structure of YOF, which means that the Eu^{3+} ions are located at sites without or deviating from inversion symmetry.[19,27,45] In addition, the higher-level $^5D_{1,2,3}$ emissions of Eu^{3+} can be easily quenched and the red emission ($^5D_0 \rightarrow {}^7F_2$) becomes dominant with increasing Eu^{3+} doping concentration, which can be proved by the emission spectrum (Figure 6b) and CIE coordinates (Figure S2, Supporting Information) for the YOF:$x$$Eu^{3+}$ samples.

The excitation spectra of YOF:Tm^{3+}/Dy^{3+} samples as shown in Figure 5c,d all consist of a broad band with a maxima at 210 and 203 nm and some weak narrow lines around 360 nm, which could be assigned to the host absorption and the typical $4f^n \rightarrow 4f^n$ intraconfiguration forbidden transitions of Tm^{3+}/Dy^{3+}, respectively.[41] The major emission peak of YOF:0.005Tm^{3+} is at 454 nm, corresponding to the transition $^1D_2 \rightarrow {}^3F_4$, on excitation with 210 nm irradiation, which results in a strong blue emission with higher color purity (point 6 in Figure S2, Supporting Information). The YOF:0.01Dy^{3+} phosphor shows a strong yellow emission (point 7 in Figure S2) on excitation at 203 nm. The emission peaks of YOF:0.01Dy^{3+} consist of a strong peak at 580 nm and a weak peak at 484 nm (Figure 5d), corresponding to the transitions $^4F_{9/2} \rightarrow {}^6H_{13/2}$ and $^4F_{9/2} \rightarrow {}^6H_{15/2}$, respectively. The transition $^4F_{9/2} \rightarrow {}^6H_{13/2}$ belongs to the hypersensitive transition with ΔJ = 2, which is strongly influenced by the outside environment of Dy^{3+}; thus, the ($^4F_{9/2} \rightarrow {}^6H_{13/2}$)/($^4F_{9/2} \rightarrow {}^6H_{15/2}$) emission ratio (Y/B) of Dy^{3+} could also be used as a probe to detect the local symmetry of the activator ions, except for the ($^5D_0 \rightarrow {}^7F_2$)/($^5D_0 \rightarrow {}^7F_1$) emission ratio of Eu^{3+}.[45,46] In the YOF system, the yellow emission $^4F_{9/2} \rightarrow {}^6H_{13/2}$ (electric dipole transition) is much stronger than the blue emission $^4F_{9/2} \rightarrow {}^6H_{15/2}$ (magnetic dipole transition), which confirmed that Dy^{3+} ions are located in an asymmetrical chemical environment.

The f–f transitions of Ho^{3+}, i.e., $^5I_8 \rightarrow {}^3H_6$ (360 nm) and $^5I_8 \rightarrow {}^5G_6$ (450 nm) and of Sm^{3+}, i.e., $^6H_{5/2} \rightarrow {}^6P_{15/2}$ (364 nm) and $^6H_{5/2} \rightarrow {}^4K_{11/2}$ (407 nm), have stronger intensity in comparison with the host absorption, as shown in Figure 5e,f, monitored at the wavelengths 545 and 608 nm, respectively.[20,47] The emission spectrum of YOF:0.005Ho^{3+} shows one dominant peak at 545 nm ($^5S_2 \rightarrow {}^5I_8$) and thus gives a green emission (point 8 in Figure S2, Supporting Information). Upon the excitation at 407 nm, YOF:0.005Sm^{3+} samples show emissions at 572 nm ($^4G_{5/2} \rightarrow {}^6H_{5/2}$), 608 nm ($^4G_{5/2} \rightarrow {}^6H_{7/2}$), and 652 nm ($^4G_{5/2} \rightarrow {}^6H_{9/2}$), respectively.

The PL intensity of Ln^{3+} as a function of their doping concentrations in YOF samples is shown in Figure S4 (Supporting Information). Generally, the concentration quenching of luminescence is due to the energy migration among the activator ions at high concentrations, during which the excitation energy will be lost at killer or quenching sites, accompanied by the decrease in the PL intensity.[5,48] The critical distance R_C between Ln^{3+} ions can be estimated by using the equation $R_C \approx 2[3V/4\pi XcN]^{1/3}$ (where V is the volume of the unit cell, N is the number of the host cations in the unit cell, and X_C is the critical concentration of doped ions). Taking Tm^{3+} for example, N = 6 and V = 235.85 Å^3, X_C is 1.5% for Tm^{3+}; therefore, the R_C value was calculated to be about 17.11 Å. In particular, for the concentration quenching of Tb^{3+}, Dy^{3+}, and Sm^{3+} luminescence is mainly caused by cross relaxation: i.e., Tb^{3+} $^5D_3 + {}^7F_6 \rightarrow {}^5D_4 + {}^7F_0$, Dy^{3+} ($^4F_{9/2}$) + Dy^{3+} ($^6H_{15/2}$) → Dy^{3+} ($^6F_{3/2}$) + Dy^{3+} ($^6F_{11/2}$) and Sm^{3+} ($^4G_{5/2}$) + Sm^{3+} ($^6H_{5/2}$) → 2Sm^{3+} ($^6F_{9/2}$).[20,41]

Cathodoluminescence Properties. The CL properties of as-prepared nanospheres YOF:Ln^{3+} (Ln = Tb, Eu, Tm, Dy, Ho, Sm) have also been investigated in detail considering their potential application in FEDs. The CL spectra of YOF:0.03Tb^{3+} samples (Figure 7a) give the characteristic transitions of Tb^{3+} with a maximum emission peak at 545 nm, producing a bright green emission, under low-voltage electron-beam excitation. The commercial phosphor ZnO:Zn exhibits green luminescence with broad band emissions at a maximum

dx.doi.org/10.1021/ic401501t | Inorg. Chem. 2013, 52, 12986–12994

at about 500 nm and has been proven to be a good candidate for an FED phosphor with low-voltage excitation.[49] As shown in Figure 7a, the integrated emission peak area of YOF:0.03Tb^{3+} is smaller than that of ZnO:Zn. However, the CL intensity of the former is higher than that of the latter.[41] In addition, the CIE coordinates of YOF:0.03Tb^{3+} and ZnO:Zn are calculated from the CL spectra to be (0.295, 0.421) and (0.219, 0.383); thus, the emission color of YOF:0.03Tb^{3+} is more saturated than that of ZnO:Zn, which could also be confirmed by their luminescence photographs as shown in Figure 7a. Thus, YOF:0.03Tb^{3+} may be a promising green phosphor for practical applications in FEDs. It is obvious that YOF:0.03Tb^{3+} nanospheres prepared at pH 2 have a higher CL intensity in comparison with other samples (pH 4) under low-voltage electron beam excitation, as shown in Figure S5 (Supporting Information). As is well-known, defects which provide nonradiative recombination routes for electrons and holes have serious drawbacks in luminescence intensity for phosphors and the large surface area results in a large number of defects.[5,50] In our system, the defect number of the former (nanospheres with diameter 170 nm) is much less than that of the latter (nanospheres with diameter 60 nm) because of the larger size. Therefore, the samples prepared at pH 2 have a higher CL intensity. Furthermore, YOF:0.07Eu^{3+}, YOF:0.01Tm^{3+}, YOF:0.015Dy^{3+}, YOF:0.01Ho^{3+}, and YOF:0.01Sm^{3+} samples give bright red, blue, yellow, green and yellowish-orange emission under the low-voltage electron beam excitation, respectively, as seen in the photographs given in Figure 7, which is beneficial for full-color FEDs.

It is anticipated that multicolor luminescence could be obtained through changing the doped Ln^{3+} ions and the corresponding concentrations, due to the simultaneous luminescence of Ln^{3+} ions, which is also confirmed by our experiments, as shown in Figure 8.[51−54] Especially for the YOF:0.001Tm^{3+},0.01Dy^{3+} samples, the characteristic transitions of Tm^{3+} ($^1D_2 \rightarrow {}^3F_4$, 455 nm) and Dy^{3+}, i.e., $^4F_{9/2} \rightarrow {}^6H_{15/2}$ (491 nm) and $^4F_{9/2} \rightarrow {}^6H_{13/2}$ (580 nm), simultaneously appear, which results in a white emission (x = 0.329, y = 0.321), as shown in the inset of Figure 8b. Furthermore, the luminescence colors in YOF:$x$$Eu^{3+}$ (Sm^{3+}),$y$$Tb^{3+}$,$z$$Tm^{3+}$ systems could be easily modulated in a broad scope, as shown by the photographs and CIE chromaticity coordinates displayed in Figure 9, which is beneficial for their use in FEDs.

As revealed in Figure 10, the CL emission intensities of YOF:0.001Tm^{3+},0.01Dy^{3+}, YOF:0.03Tb^{3+}, YOF:0.07Eu^{3+}, YOF:0.01Tm^{3+}, and YOF:0.01Ho^{3+} increase not only with an increase in the accelerating voltage but also with the increase of the filament current. Furthermore, with an increase of the accelerating voltage and filament current, no obvious saturation effect appears. The electron penetration depth L (Å) of YOF:Ln^{3+} phosphors could be calculated on the basis of the formula L (Å) = 250 $(A/\rho)(E/Z^{1/2})^n$, where $n = 1.2/(1 - 0.29 \log Z)$, A is the atomic or molecular weight, ρ is the bulk density, E is the excitation energy (keV), and Z is the atomic number or the number of electrons per molecule.[55,56] Because the penetration depth of the electron beam into the phosphor body increases with an increase of accelerating voltage and filament current, more Tb^{3+}, Eu^{3+}, Tm^{3+}, Dy^{3+}, and Ho^{3+}, Sm^{3+} ions could be excited, and so the CL intensity increases.

CONCLUSIONS

Multiform YOF:Ln^{3+} (Ln = Tb, Eu, Tm, Dy, Ho, Sm) nano-/microstructures, including nanospheres, nanorod bundles, and microspindles, have been synthesized via a facile modified urea-based homogeneous precipitation (UBHP) technique followed by a heat treatment. The influences of pH values and fluoride sources on the morphologies of YOF have been investigated in detail. Moreover, various luminescence colors could be obtained easily in YOF:Ln^{3+} nanospheres because of the characteristic f−f transitions and the simultaneous luminescence of Ln^{3+} ions, under UV light and low-voltage electron beam excitation. In comparison with the commercial phosphor ZnO:Zn, the YOF:0.03Tb^{3+} samples exhibit superior green luminescence properties to a degree, which is beneficial for improving display quality. In addition, under low-voltage electron beam excitation, the nanosphere samples (diameter about 170 nm) prepared at pH 2 have a higher CL intensity than the samples prepared at pH 4 (diameter about 60 nm) due to the lower defect concentration. Because of their low raw-materials cost, strong CL intensity, superior stability, good CIE chromaticity, and ease of mass production, these materials have great promise for applications in FEDs.

ASSOCIATED CONTENT

Supporting Information

Figures and a table giving TG-DSC curves of as-prepared precursor samples at pH 2 using KF as F^- source, CIE chromaticity diagrams for (1) YOF:0.005Tb^{3+}, (2) YOF:0.03Tb^{3+}, (3) YOF:0.10Tb^{3+}, (4) YOF: 0.01Eu^{3+}, (5) YOF:0.10Eu^{3+}, (6) YOF:0.005Tm^{3+}, (7) YOF:0.01Dy^{3+}, (8) YOF:0.005Ho^{3+}, and (9) YOF:0.005Sm^{3+} under UV excitation, the diffuse reflectance spectrum of the YOF product obtained by calcining the as-prepared precursor at 600 °C in air for 3 h, the PL intensity of Ln^{3+} (Ln = Tb, Eu, Tm, Dy, Ho, Sm) as a function of its doping concentration in the YOF host, CL spectra of YOF:0.03Tb^{3+} samples prepared at pH 2 and 4, and CIE color coordinates (x, y) of ZnO:Zn and YOF:Ln^{3+} (Ln = Tb, Eu, Tm, Dy, Ho, Sm) under a low-voltage electron beam (accelerating voltage 3.0 kV; filament current 90 mA). This material is available free of charge via the Internet at http://pubs.acs.org.

AUTHOR INFORMATION

Corresponding Author

*E-mail: jlin@ciac.ac.cn.

Notes

The authors declare no competing financial interest.

ACKNOWLEDGMENTS

This project was financially supported by the National Natural Science Foundation of China (Grants NSFC 51332008, 51172227, and 21221061) and the National Basic Research Program of China (Grant 2010CB327704, 2014CB643803), and the Joint Funds of the National Natural Science Foundation of China and Guangdong Province (Grant No. U13012038).

REFERENCES

(1) Höppe, H. A. *Angew. Chem., Int. Ed.* **2009**, *48*, 3572−3582.
(2) Xie, R. J.; Hirosaki, N.; Sakuma, K.; Yamamoto, Y.; Mitomo, M. *Appl. Phys. Lett.* **2004**, *84*, 5404−5406.
(3) Dai, Q.; Foley, M. E.; Breshike, C. J.; Lita, A.; Strouse, G. F. *J. Am. Chem. Soc.* **2011**, *133*, 15475−15486.
(4) Ye, S.; Xiao, F.; Pan, Y. X.; Ma, Y. Y.; Zhang, Q. Y. *Mater. Sci. Eng., R.* **2010**, *71*, 1−34.

(5) Li, G.; Hou, Z.; Peng, C.; Wang, W.; Cheng, Z.; Li, C.; Lian, H.; Lin, J. *Adv. Funct. Mater.* **2010**, *20*, 3446−3456.
(6) Wang, P.; Wang, Y.; Tong, L. *Light Sci. Appl.* **2013**, *2*, e102.
(7) Huang, C.-H.; Chan, T.-S.; Liu, W.-R.; Wang, D.; Chiu, Y.-C.; Yeh, Y.-T.; Chen, T.-M. *J. Mater. Chem.* **2012**, *22*, 20210−20216.
(8) Liu, W.-R.; Huang, C.-H.; Yeh, C.-W.; Tsai, J.-C.; Chiu, Y.-C.; Yeh, Y.-T.; Liu, R.-S. *Inorg. Chem.* **2012**, *51*, 9636−9641.
(9) Psuja, P.; Hreniak, D.; Strek, W. *J. Nanomater.* **2007**, *2007*, 81350.
(10) Li, J.-G.; Li, X.; Sun, X.; Ikegami, T.; Ishigaki, T. *Chem. Mater.* **2008**, *20*, 2274−2281.
(11) Mao, Y.; Tran, T.; Guo, X.; Huang, J. Y.; Shih, C. K.; Wang, K. L.; Chang, J. P. *Adv. Funct. Mater.* **2009**, *19*, 748−754.
(12) Hirai, T.; Hirano, T.; Komasawa, I. *J. Mater. Chem.* **2000**, *10*, 2306−2310.
(13) Li, J. G.; Li, X.; Sun, X.; Ishigaki, T. *J. Phys. Chem. C* **2008**, *112*, 11707−11716.
(14) Du, Y.-P.; Zhang, Y.-W.; Sun, L.-D.; Yan, C.-H. *J. Am. Chem. Soc.* **2009**, *131*, 3162−3163.
(15) Sun, X.; Zhang, Y. W.; Du, Y. P.; Yan, Z. G.; Si, R.; You, L. P.; Yan, C. H. *Chem. Eur. J.* **2006**, *13*, 2320−2332.
(16) Kort, K. R.; Banerjee, S. *Inorg. Chem.* **2011**, *50*, 5539−5544.
(17) Huang, X.; Han, S.; Huang, W.; Liu, X. *Chem. Soc. Rev.* **2013**, *42*, 173−201.
(18) Yi, G.; Peng, Y.; Gao, Z. *Chem. Mater.* **2011**, *23*, 2729−2734.
(19) Hölsä, J.; Kestilä, E. *J. Chem. Soc., Faraday Trans.* **1995**, *91*, 1503−1509.
(20) Shang, M.; Geng, D.; Kang, X.; Yang, D.; Zhang, Y.; Lin, J. *Inorg. Chem.* **2012**, *51*, 11106−11116.
(21) Ding, M.; Lu, C.; Cao, L.; Ni, Y.; Xu, Z. *Opt. Mater.* **2013**, *35*, 1283−1287.
(22) Yang, R.; Qin, G.; Zhao, D.; Zheng, K.; Qin, W. *J. Fluorine Chem.* **2012**, *140*, 38−42.
(23) Feng, W.; Sun, L.-D.; Zhang, Y.-W.; Yan, C.-H. *Coord. Chem. Rev.* **2010**, *254*, 1038−1053.
(24) Mann, A.; Bevan, D. *Acta Crystallogr., Sect. B* **1970**, *26*, 2129−2131.
(25) Grzyb, T.; Węcławiak, M.; Lis, S. *J. Alloys Compd.* **2012**, *539*, 82−89.
(26) Shannon, R. D. *Acta Crystallogr., Sect. A* **1976**, *32*, 751−767.
(27) Hölsä, J.; Piriou, B.; Räsänen, M. *Spectrochim. Acta, Part A* **1993**, *49*, 465−470.
(28) Shang, M.; Li, G.; Kang, X.; Yang, D.; Geng, D.; Peng, C.; Cheng, Z.; Lian, H.; Lin, J. *Dalton Trans.* **2012**, *41*, 5571−5580.
(29) Zhang, X.; Yang, P.; Wang, D.; Xu, J.; Li, C.; Gai, S.; Lin, J. *Cryst. Growth Des.* **2011**, *12*, 306−312.
(30) Fang, Y. P.; Xu, A. W.; You, L. P.; Song, R. Q.; Yu, J. C.; Zhang, H. X.; Li, Q.; Liu, H. Q. *Adv. Funct. Mater.* **2003**, *13*, 955−960.
(31) Wang, X.; Sun, X. M.; Yu, D.; Zou, B. S.; Li, Y. *Adv. Mater.* **2003**, *15*, 1442−1445.
(32) Wang, X.; Li, Y. *Chem. Eur. J.* **2003**, *9*, 5627−5635.
(33) Aiken, B. A. R.; Hsu, W. P.; MatijeviĆ, E. *J. Am. Ceram. Soc.* **1988**, *71*, 845−853.
(34) Matijevic, E. *Chem. Mater.* **1993**, *5*, 412−426.
(35) Liu, B.; Aydil, E. S. *J. Am. Chem. Soc.* **2009**, *131*, 3985−3990.
(36) Vayssières, L.; Chanéac, C.; Tronc, E.; Jolivet, J. P. *J. Colloid Interface Sci.* **1998**, *205*, 205−212.
(37) Jolivet, J.-P.; Froidefond, C.; Pottier, A.; Chanéac, C.; Cassaignon, S.; Tronc, E.; Euzen, P. *J. Mater. Chem.* **2004**, *14*, 3281−3288.
(38) Adachi-Pagano, M.; Forano, C.; Besse, J. P. *J. Mater. Chem.* **2003**, *13*, 1988−1993.
(39) Wang, M.; Huang, Q.-L.; Hong, J.-M.; Chen, X.-T.; Xue, Z.-L. *Cryst. Growth Des.* **2006**, *6*, 2169−2173.
(40) Li, C.; Yang, J.; Quan, Z.; Yang, P.; Kong, D.; Lin, J. *Chem. Mater.* **2007**, *19*, 4933−4942.
(41) Zhang, Y.; Geng, D.; Shang, M.; Zhang, X.; Li, X.; Cheng, Z.; Lian, H.; Lin, J. *Dalton Trans.* **2013**, *42*, 4799−4808.
(42) Lin, J.; Su, Q. *J. Mater. Chem.* **1995**, *5*, 1151−1154.
(43) Blasse, G.; Bril, A. *Philips Res. Rep.* **1967**, *22*, 481−504.
(44) Liu, X.; Li, C.; Quan, Z.; Cheng, Z.; Lin, J. *J. Phys. Chem. C* **2007**, *111*, 16601−16607.
(45) Yu, M.; Lin, J.; Fang, J. *Chem. Mater.* **2005**, *17*, 1783−1791.
(46) Su, Q.; Pei, Z.; Chi, L.; Zhang, H.; Zhang, Z.; Zou, F. *J. Alloys Compd.* **1993**, *192*, 25−27.
(47) Stouwdam, J. W.; van Veggel, F. C. *Nano Lett.* **2002**, *2*, 733−737.
(48) Dexter, D. L.; Schulman, J. H. *J. Chem. Phys.* **1954**, *22*, 1063−1070.
(49) Geng, D.; Li, G.; Shang, M.; Peng, C.; Zhang, Y.; Cheng, Z.; Lin, J. *Dalton Trans.* **2012**, *41*, 3078−3086.
(50) Yu, L.; Song, H.; Liu, Z.; Yang, L.; Zheng, S. L. Z. *J. Phys. Chem. B* **2005**, *109*, 11450−11455.
(51) Park, J. K.; Choi, K. J.; Kim, K. N.; Kim, C. H. *Appl. Phys. Lett.* **2005**, *87*, 031108.
(52) Li, H. C.; Lin, Y. P.; Chou, P. T.; Cheng, Y. M.; Liu, R. S. *Adv. Funct. Mater.* **2007**, *17*, 520−530.
(53) He, G.; Guo, D.; He, C.; Zhang, X.; Zhao, X.; Duan, C. *Angew. Chem., Int. Ed.* **2009**, *48*, 6132−6135.
(54) Dexpert-Ghys, J.; Mauricot, R.; Caillier, B.; Guillot, P.; Beaudette, T.; Jia, G.; Tanner, P. A.; Cheng, B.-M. *J. Phys. Chem. C* **2010**, *114*, 6681−6689.
(55) Liu, X.; Yan, L.; Lin, J. *J. Phys. Chem. C* **2009**, *113*, 8478−8483.
(56) Feldman, C. *Phys. Rev.* **1960**, *117*, 455−459.